Journal of Solid State Chemistry 183 (2010) 1326–1333

Contents lists available at ScienceDirect

Journal of Solid State Chemistry

journal homepage: www.elsevier.com/locate/jssc

Highly ordered Ti-SBA-15: Efficient H_2 adsorbent and photocatalyst for eco-toxic dye degradation

Swapan K. Das, Manas K. Bhunia, Asim Bhaumik *

Department of Materials Science, Indian Association for the Cultivation of Science, 2A & B Raja S.C. Mullick Road, Jadavpur, Kolkata 700 032, India

ARTICLE INFO

Article history:
Received 14 January 2010
Received in revised form
2 March 2010
Accepted 10 April 2010
Available online 27 April 2010

Keywords:
Gas adsorption
Mesoporous material
Photocatalysis
Ti-SBA-15
H_2 storage
Titanium silicate

ABSTRACT

Highly ordered 2D-hexagonal mesoporous titanium silicate Ti-SBA-15 materials (space group *p6mm*) have been synthesized hydrothermally in acidic medium employing amphiphilic tri-block copolymer, Pluronic F127 as structure directing agent. Samples are characterized by powder X-ray diffraction, transmission electron microscopy, scanning electron microscopy, FT IR spectroscopy, UV–visible diffuse reflectance measurements, N_2 adsorption/desorption and TG-DTA analysis. XRD and TEM results suggested the presence of highly ordered mesophase with hexagonal pore arrangements. BET surface area for Ti-SBA-15 ($924\,m^2\,g^{-1}$) is considerably higher than the pure silica SBA-15 ($611\,m^2\,g^{-1}$) prepared following the same synthetic route. UV–visible and FT-IR studies suggested the incorporation of mostly tetrahedral titanium (IV) species, along with some six-coordinated sites in the silicate network. This material shows very good H_2 adsorption capacity at higher pressure and excellent catalytic activity in the photocatalytic degradation of ecologically abundant dye methylene blue.

© 2010 Elsevier Inc. All rights reserved.

1. Introduction

Mesoporous materials have attracted widespread interest in many frontier areas of science due to their unique structural features like exceptionally high surface area, uniform and well-defined pore topology since the first synthesis of MCM-41 in 1992 [1]. Supramolecular templating approach for the synthesis of these materials with the aid of ionic and non-ionic surfactants has been extended to prepare mesoporous materials of metal oxides [2,3], sulphides [4–6], phosphates [7], metal-anchored [8] and metal-incorporated molecular sieves [9,10]. These materials are utilized efficiently in adsorption [11], optoelectronics [12], magnetic [13], sensing technology [14], photovoltaics [15] catalysis [16–18] and so on. A variety of mesoporous titanium silicates like Ti-MCM-41 [16,17] and Ti-MCM-48 [18] have been synthesized, which show remarkable catalytic activity in a series of liquid phase partial oxidation reactions in the presence of peroxides as oxidant. Thus, mesoporous titanium silicate, where Ti^{4+} ion isomorphously substitutes the Si^{4+} in the silicate framework is of great interest from both academic and industrial viewpoints [18]. However, it is very difficult to incorporate titanium into silicate framework under acidic medium by using amphiphilic tri-block copolymer as template through co-condensation of silicon and titanium alkoxide precursors due to different rate of hydrolysis of both alkoxide precursors [19]. Incorporation of titanium into silicate framework in the presence of amphiphilic tri-block copolymer through a grafting method under aqueous acidic medium has been reported [20]. Although there are some reports on direct preparation of Ti-SBA-15 using modified procedures [21] synthesis of catalytically active Ti-SBA-15 still remains a big challenge.

Both cationic and anionic surfactants are frequently used to prepare ordered mesoporous titanium silicates with relatively thin walls in the alkaline conditions. On the other hand, non-ionic amphiphilic block copolymers are frequently used in acidic medium to direct the formation of mesostructures with larger pore size, thicker wall (3–6 nm) and superior hydrothermal stabilities [22]. Thus, it is highly desirable to develop a new synthetic protocol to solve this problem through optimization of pH, ionic strength of the medium and the mode of addition of titanium source in the synthesis gel in presence of amphiphilic surfactant, where cooperative assembly process between tri-block copolymer and the inorganic precursor through hydrogen bonding in aqueous acidic medium is the key step for the success of the synthesis.

In this context it is pertinent to mention that nanoporous materials show excellent hydrogen uptake at higher applied pressure [23]. This is one of the major research interests for the fruitful utilization of hydrogen energy in the mobile systems. Most convenient way to enhance the H_2 adsorption capacity for a particular class of material is to increase the internal surface area. Environmental pollution caused by industrial effluents is another major concern today. Textile and other related industrial processes released several organic dyes, which is one of the major water pollutants. Titanium dioxide is one of the most well-known

* Corresponding author. Fax: +91 33 2473 2805.
E-mail address: msab@iacs.res.in (A. Bhaumik).

0022-4596/$ - see front matter © 2010 Elsevier Inc. All rights reserved.
doi:10.1016/j.jssc.2010.04.015

semiconductor photocatalysts for the photocatalytic degradation of several organic dyes. It is widely being used for its high stability under hazardous conditions together with excellent semiconductor characteristics. Titanium containing nanostructured materials have attracted special interest in this regard and their photocatalytic activity can be further improved by enhancing the number of active sites per unit area [24–26]. However, there are only few reports on the use of titanium incorporated SBA-15 in photocatalytic degradation of organic dyes [27,28]. Herein, we report the generalized synthesis of Ti-SBA-15, where the introduction of very small amount of titanium species into mesoporous silicate framework could result into much higher surface area ($924\,m^2\,g^{-1}$) in comparison to purely silicious SBA-15 ($611\,m^2\,g^{-1}$) following similar synthesis method. Ti-incorporation in the mesoporous framework resulted in more H_2 adsorption and excellent activity in the photocatalytic degradation of organic dye under UV visible light irradiation.

2. Experimental section

2.1. Chemicals

Non-ionic surfactant pluronic F127 ($M_{av}=12600$, $EO_{106}PO_{70}EO_{106}$), was used as the structure-directing agent, 1,2,4-trivinylcyclohexane (TVCH) as co-surfactant and tetraethyl orthosilicate (TEOS) and titanium(IV) tetrabutoxide (TBOT) were used as a silica and titanium sources, respectively. All these chemicals were purchased from Sigma-Aldrich. Hydrochloric acid (HCl) and potassium chloride (KCl) obtained from Merck were used to maintain the desired pH and ionic strength in the synthesis gels. All chemicals were used without further purification.

2.2. Synthesis

2.2.1. Synthesis of pure SBA-15

In a typical synthesis, amphiphilic tri-block copolymer pluronic F127 (1.0 g) was dissolved in 30 ml 2.36(N) aqueous hydrochloric acid (HCl) solution. After dissolving, 2.5 g potassium chloride (KCl) was added to the mixture. Then the mixture was stirred at room temperature for 2 h. Then 1.3 g 1,2,4-trivinylcyclohexane was added slowly into it and allowed to stir for overnight and total solution becomes milky. Then it was aged for 1 day at ambient temperature. After 1 day, 2.33 g tetraethyl orthosilicate was added slowly to the micellar solution and allowed to stir for 4 h. After that the mixture was covered and aged for 7 days at room temperature. Then it was transferred into an autoclave, aged at 373 K for 24 h. The resultant solid was filtered, washed with distilled water and dried at 333 K. This as-synthesized SBA-15 material was calcined by slowly increasing the temperature to 823 K ($1\,K\,min^{-1}$ ramping rate) and by heating at 823 K for 5 h in the presence of air. After calcination we have obtained template-free large mesoporous SBA-15 materials.

2.2.2. Synthesis of pure Ti- SBA-15

Amphiphilic tri-block copolymer pluronic F127 (1 g) was added to 30 ml 2.36(N) aqueous hydrochloric acid (HCl) under vigorous stirring and was allowed to stir until dissolution. After dissolving, 2.5 g potassium chloride (KCl) was added to the mixture. Then the mixture was stirred at room temperature for 2 h. Then 1.3 g 1,2,4-trivinylcyclohexane was added slowly into it and allowed to stir for overnight. Then it was aged for 1 day at ambient temperature. After 1 day, 2.33 g tetraethyl orthosilicate was added slowly to the micellar solution and allowed to stir for 4 h. Then 0.20 g titanium (IV) butoxide [$Ti(OC_4H_9)_4$] taken in 2 ml absolute ethanol was added to that solution under vigorous stirring and total mixture was allowed to stir again for 4 h. After that the mixture was covered and aged for 7 days at room temperature. Then it was transferred into an autoclave, aged at 373 K for 24 h. The resultant solid was filtered, washed with distilled water and dried at 333 K. This as-synthesized Ti-SBA-15 material was calcined by slowly increasing the temperature to 823 K ($1\,K\,min^{-1}$ ramping rate) and by heating at 823 K for 5 h in the presence of air. After these treatments we obtained template-free large mesoporous Ti-SBA-15 suitable to carry out adsorption and catalytic studies.

2.3. Characterization techniques

Powder X-ray diffraction patterns of the samples were obtained with a Bruker AXS D8 Advanced diffractometer using Cu $K\alpha$ ($\lambda=0.15406$ nm) radiation. Nitrogen adsorption/desorption isotherms were obtained using a BEL Japan Inc. Belsorp–HP surface area analyzer at 77 K. Prior to gas adsorption, all the samples were degassed for 6 h at 423 K. Hydrogen adsorption/desorption were obtained using Belsorp–HP machine under high H_2 pressure at 77 K. Transmission electron microscopic images were recorded on a JEOL 2010 TEM operated at 200 kV. SEM images in a JEOL JEM 6700F field emission scanning electron microscope were used for the determination of morphology of the particles. UV–visible diffuse reflectance spectra were recorded on a Shimadzu UV 2401PC with an integrating sphere attachment. $BaSO_4$ was used as background standard. FT-IR spectra of these samples were recorded using a Nicolet MAGNA-FT IR 750 Spectrometer Series II. Thermogravimetry (TG) and differential thermal analysis (DTA) were carried out in a TA Instruments SDT Q-600 thermal analyzer. Photodegradation experiments were performed with a photocatalytic reactor system. A 450 W medium-pressure mercury-vapor lamp (from Hanovia) used as the radiation source was placed inside the quartz tube. The lamp and the tube were immersed in the photoreactor cell, which is made up of Pyrex-glass. The reactor was filled with 250 ml (12 mg/L) solution of dye and 100 mg catalyst. The temperature of the whole reactor was maintained at 298 K by using cold-water circulation. The reaction mixture was stirred using a magnetic stirrer to keep the suspension homogeneous.

3. Results and discussion

3.1. Powder X-ray Diffraction

The small-angle powder X-ray diffraction (XRD) patterns of the as-synthesized and calcined mesoporous Ti-SBA-15 materials synthesized by using tri-block copolymer F127 as a structure directing agent are shown in Fig. 1. All the materials show four well-resolved diffraction peaks in the region of $2\theta=0.6-2.07$, which can be indexed to the 100, 110, 200 and 210 reflections [1] corresponding to a two-dimensional hexagonal mesostructure with space group *p6mm* and high structural periodicity. After calcination, the first diffraction peak is shifted to higher angle ($2\theta=0.62^\circ$ before calcination, and $2\theta=0.65^\circ$ after calcination) and corresponding *d* spacing also reduced from 14.2 to 13.6 nm. From these powder XRD patterns we can notice that Ti-SBA-15 synthesized at higher temperature (373 K) is highly ordered with sharp and intense peaks than that synthesized at lower temperature (343 K). This high ordering at higher synthesis temperature may be attributed to the better condensation between silanol and titanium centers. These materials on calcinations at 823 K result no noticeable shrinkage of pore

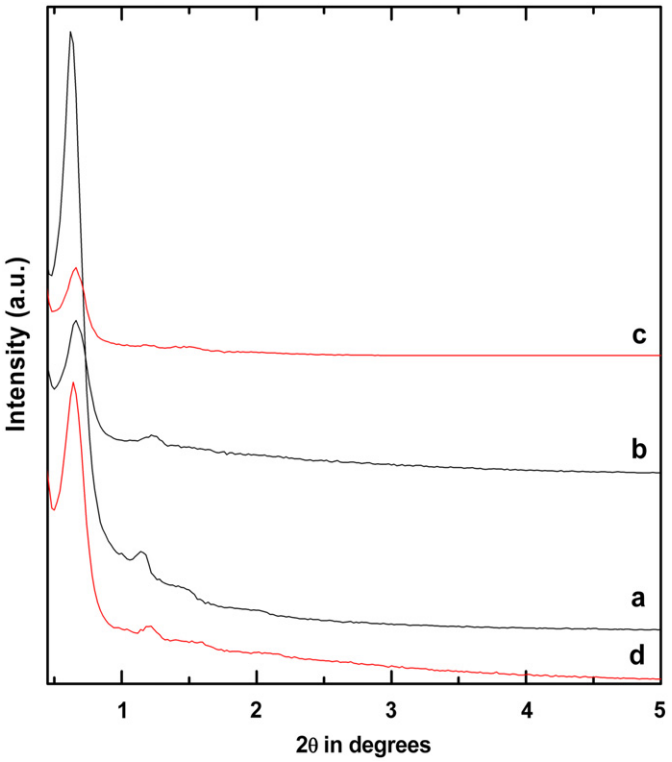

Fig. 1. Small-angle powder XRD patterns of Ti-SBA-15: as-synthesized at 373 K (a) calcined at 773 K (b), as-synthesized at 343 K (c) and calcined at 773 K (d).

width and decline in mesostructure regularity, indicating high thermal stability of the Ti-SBA-15 materials synthesized herein. Further, the wide-angle XRD pattern (not shown here) shows no higher order diffraction peak in either of the as-synthesized and calcined samples, indicating the amorphous nature of the pore walls and absence of any extra-framework TiO_2 phases. Hence, higher synthesis temperature influences the formation of more highly ordered and thermally stable Ti-SBA-15 material.

3.2. Transmission and scanning electron microscopy

Representative TEM images of mesoporous Ti-SBA-15 and SBA-15 samples are shown in Figs. 2a and 2b, respectively. In these images low electron density spots (pores) are seen throughout the respective specimens. The uniform and long range ordered large mesopores are clearly observed from these TEM images. TEM images and corresponding FFT diffractograms (insets of Figs. 2a and 2b) are recorded in the [100] direction indicates long range ordering and hexagonally arranged pores [29–31]. In the case of SBA-15 materials, pores are uniform in size of ca. 9.2 nm and the wall-thickness varies from 5.0 to 5.8 nm. Whereas, in case of Ti-SBA-15 pores are also uniform in size of about 10.3–10.5 nm and wall thickness varies from 4.0 to 4.5 nm. Thus, incorporation of titanium into the SBA-15 silica framework makes the pore walls slimmer than the pure SBA-15. Consequently, the material becomes lighter. Scanning electron microscope (SEM) images (shown in Fig. 3) reveal that as-synthesized samples are composed of plate-like uniform particles of about 0.34 μm in thickness and 3–4.5 μm in size. All of these particles have the shape of a hexagonal plate consisting of 8 well-defined faces. These hexagonal plates have been agglomerated together to form a large size of spheres with diameters ranging from 13 to 14.5 μm.

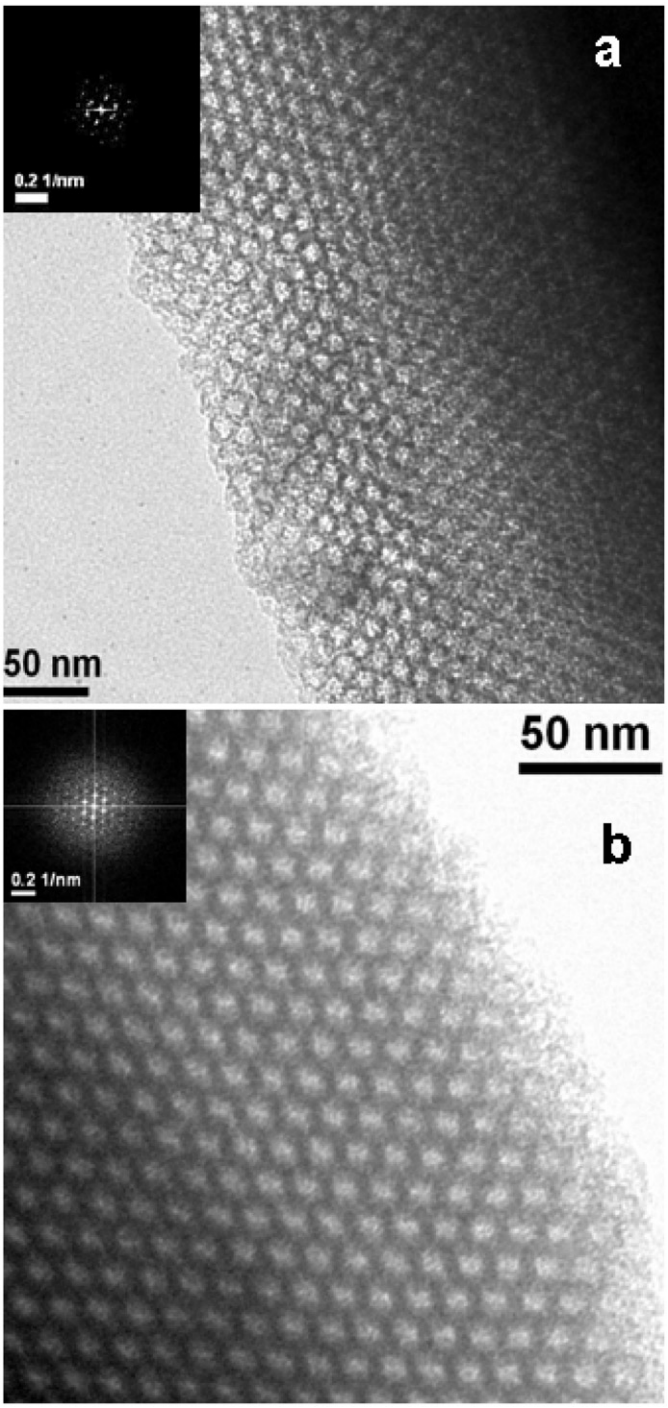

Fig. 2. TEM images of calcined mesoporous Ti-SBA-15 (a, sample 1) and pure silica SBA-15 (b) materials seen through the direction perpendicular to the pore axis. FFT patterns are shown in the insets.

3.3. N_2 sorption

Nitrogen-sorption studies carried out on the calcined mesoporous SBA-15 and Ti-SBA-15 materials at 77 K, show type-IV adsorption–desorption isotherms (Fig. 4) with a very large H2 type hysteresis loop in the P/P_0 range from 0.60 to 0.82. These isotherms suggest large uniform mesopores connected by windows of small size cage-like pores and confirming that the samples are mesoporous [29]. Calcined mesoporous SBA-15 (Fig. 4a) and Ti-SBA-15 (Fig. 4b and 4c) materials exhibit sharp inflections in the P/P_0 range from 0.60 to 0.82. This is the

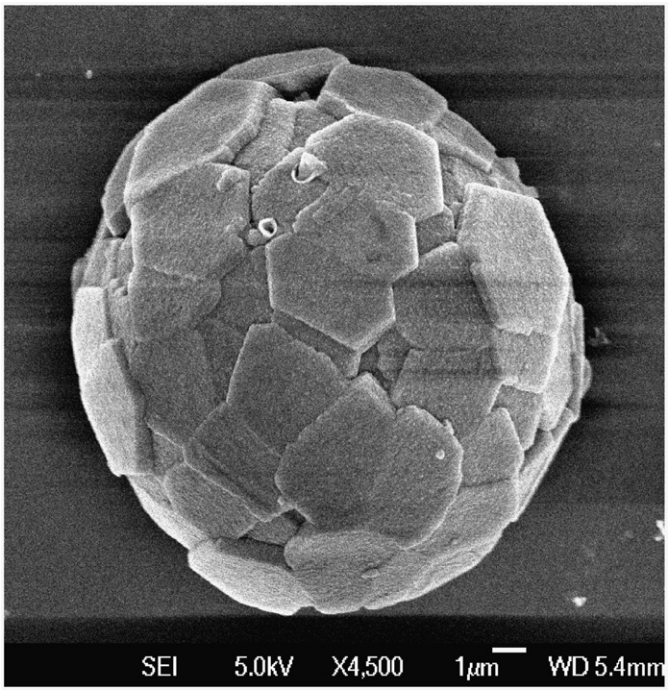

Fig. 3. FE-SEM image of mesoporous Ti-SBA-15 (sample 1).

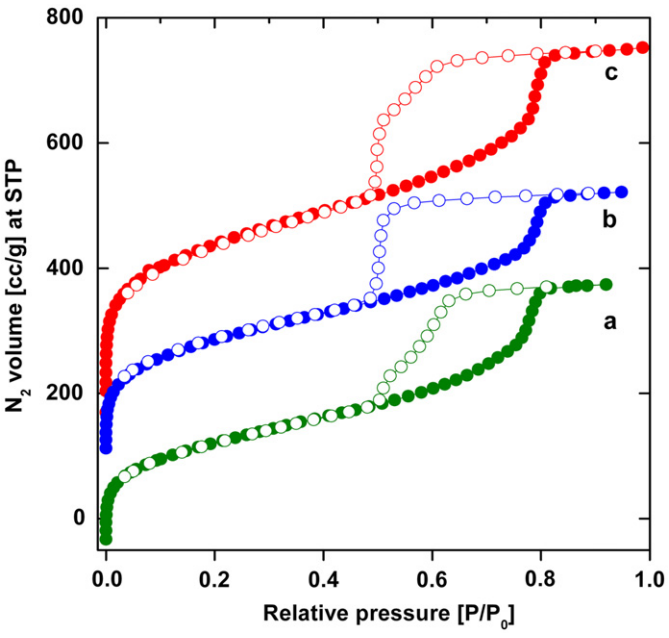

Fig. 4. N_2 adsorption/desorption isotherms of mesoporous Ti-SBA-15 and SBA-15: pure silicious SBA-15 (a), mesoporous Ti-SBA-15 synthesized at 343 K (b) and Ti-SBA-15 synthesized at 373 K (c) measured at 77 K. Adsorption points are marked by filled circles and desorption points by empty circles.

characteristic of capillary condensation within uniform pores. The P/P_0 position of the inflection points is clearly related to pore-widths in the mesopore range and the sharpness of these steps indicates the distributions of the mesopores are uniform in size [29]. Brunauer–Emmett–Teller (BET) surface area, average pore diameter and pore volume, of these samples estimated from their respective adsorption–desorption isotherms are given in Table 1. The BET surface areas of the calcined mesoporous SBA-15, Ti-SBA-15 (synthesized at 373 and 343 K) are 611, 924, 661 $m^2 g^{-1}$, respectively. Here, BET surface areas of Ti-SBA-15 samples are

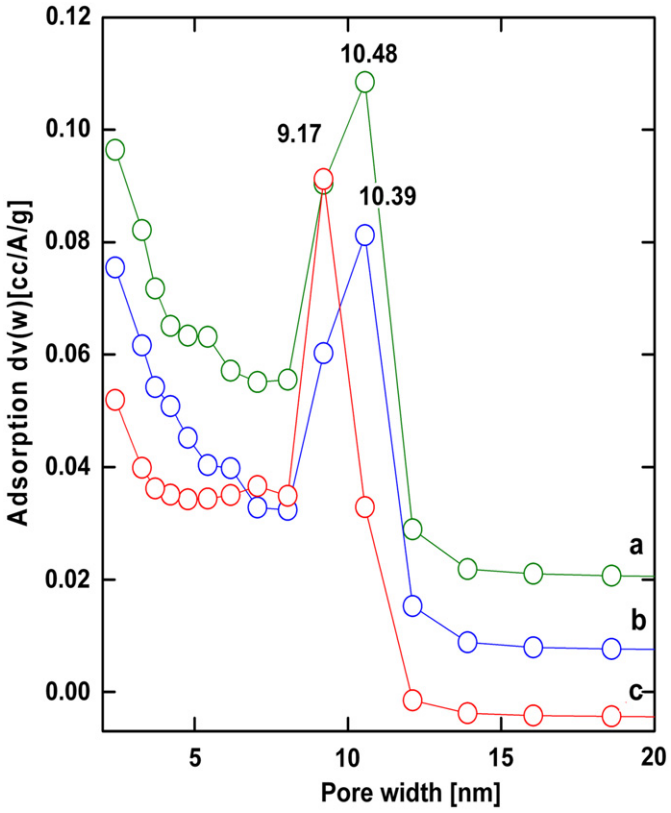

Fig. 5. BJH pore size distributions of SBA-15 (a), Ti-SBA-15 synthesized at 343 K (b) and Ti-SBA-15 synthesized at 373 K (c).

sufficiently higher than pure SBA-15. Titanium incorporation into SBA-15 framework makes the pore walls slimmer than pure SBA-15, which is reflected from their surface areas and this has been confirmed from their respective TEM images also. Although for both samples Si/Ti mole ratio of the gel is 20, sample synthesized at 373 K possesses relatively large amount of Ti than that synthesized at 343 K (Table 1). Pore size distribution of these samples estimated employing the BJH method is shown in Fig. 5a–c. Estimated pore widths for these samples are 9.17, 10.39 and 10.48 nm, which agree quite well with the pore widths obtained from the TEM image analysis and XRD studies.

3.4. H_2 adsorption studies

The H_2 adsorption/desorption of mesoporous pure silica SBA-15 and Ti-SBA-15 materials are shown in Fig. 6. H_2 adsorption/desorption are measured at 77 K at pressures of up to 20 bar and saturation adsorption has been achieved at this pressure. From this figure, it is clear that pure silica mesoporous SBA-15 (in Fig. 6a) materials adsorb 0.90 wt% hydrogen at 20 bar, whereas Ti-SBA-15 (Fig. 6b) sample under similar condition adsorbs ca. 1.30 wt% hydrogen. It is pertinent to mention that doping of Ti over different carbon nanostructures is known to enhance the H_2 adsorption capacity of that material [32]. The reason of higher H_2 uptake in these materials is attributed to weak interactions of the adsorbed H_2 with the Ti sites under high pressure. Here, we have seen that the presence of Ti-sites in the Ti-SBA-15 enhances the H_2 adsorption amount by ca. 45% with reference to pure silica SBA-15. Thus, H_2 adsorption capacity of our Ti-SBA-15 is approximately 6% larger than the difference in surface areas of the two materials. Very recently Acatrinei et al. [33] also observed a similar nearly twice the amount of hydrogen

Table 1
Physico-chemical properties of mesoporous SBA-15 and mesoporous Ti-BA-15 materials.

Sample name	Synthesis temperature (K)	Si/Ti mole ratio in the product	Surface area ($m^2 g^{-1}$)	Pore width (nm)	Pore volume ($cc g^{-1}$)
SBA-15	373	–	611	9.72	0.6336
Ti-SBA-15 (1)	373	39.5	924	10.48	0.8568
Ti-SBA-15 (2)	343	47.4	661	10.39	0.6265

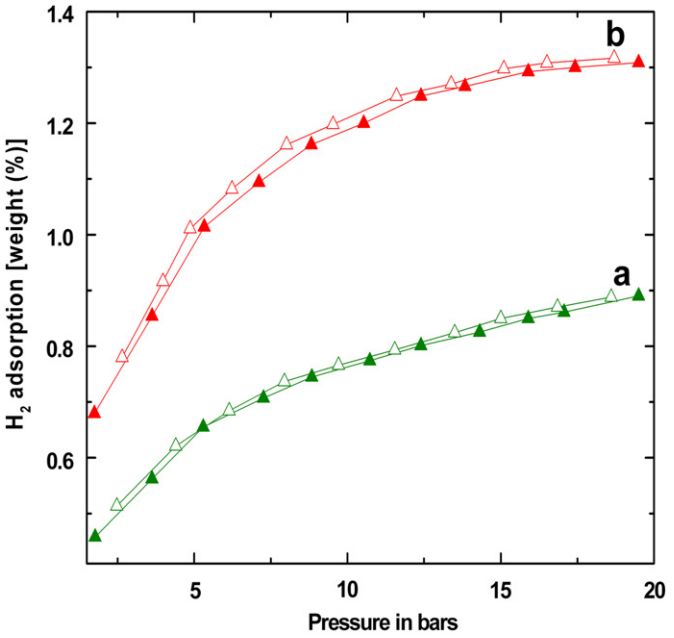

Fig. 6. H_2 adsorption/desorption of SBA-15 (a) and Ti-SBA-15 (b, sample 1) measured at 77 K.

adsorption at a pressure of 25 bar for Ti-rich SBA-15 vis-à-vis pure silica SBA-15 synthesized by using P123 as template. At 77 K and 25 bar pressure their Ti-SBA-15 (BET surface area 835 $m^2 g^{-1}$) adsorbs nearly 0.95 wt% compared to 1.3 wt% for our Ti-SBA-15 sample (more highly ordered sample with BET surface area 924 $m^2 g^{-1}$) at 20 bar pressure. Adsorption of hydrogen in SBA-15 is controlled by the relatively weak interaction of H_2 with hydroxyl groups and oxygen atoms that present at the surface of the pores in SBA-15 materials. Presence of these sites is also responsible for high H_2 uptake in Ti-SBA-15 material. Furthermore, we propose that H_2 molecules in the vicinity of the Ti site form bridging hydroxyls (e.g., Ti–O(H)–Si) and additional Ti–OH groups at the surface of Ti-SBA-15 helps to form these weak interactions under high hydrogen pressure [33]. Higher adsorption capacity has been previously ascribed to the loading of titanium atoms in the SBA-15 material as evidenced from the interaction of hydrogen with Ti in Ti-SBA-15 noticed through neutron vibrational spectroscopy [33]. Thus, high H_2 uptake in Ti-SBA-15 over SBA-15 could be attributed to the increase in surface area as well as loading of Ti in this mesoporous material.

3.5. UV–vis absorption

Coordination and the bonding of the Ti sites to the silica framework are very important to explore the applications of titanium silicates and this can be investigated spectroscopically. UV–visible spectroscopy is used for characterizing the coordination mode of the titanium centers in mesoporous Ti-SBA-15. In Figs. 7a and 7b UV–visible diffuse reflectance spectra of

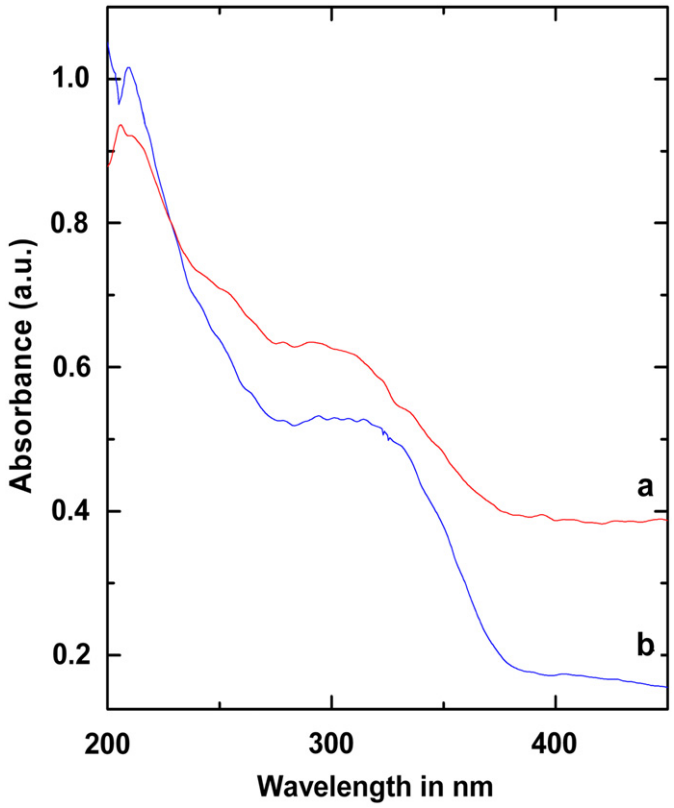

Fig. 7. UV–vis diffuse reflectance spectrum of the calcined Ti-SBA-15 (a, sample 1) and Ti-SBA-15 (b, sample 2) materials.

mesoporous Ti-SBA-15 samples 1 and 2 are shown. Sharp absorption peak centered at 210 nm is observed for both samples. This could be attributed to the presence of Ti species in tetrahedral coordination in these frameworks [21,31]. This band at lower wavelength can be assigned to an electronic charge-transfer transition associated with an isolated Ti(IV) framework site in tetrahedral coordination [34]. Further, a broad absorption peak is observed at about 290–320 nm. This could be attributed to the presence of octahedral Ti^{4+} sites in the framework. Synthesis of Ti-SBA-15 under strongly acidic pH (strong acid condition favors positively charged hexa-coordinated Ti^{4+} species) could be responsible for higher coordination. This higher coordination number for the Ti-sites is not suitable for the catalytic activity of a mesoporous titanium silicate material in liquid phase oxidation reactions in the presence of peroxide oxidants [34–36]. However, higher coordination and thus lower band gap in turn can be helpful for the photocatalytic activity of Ti-SBA-15 under UV visible light irradiation.

3.6. FT-IR spectroscopy

In Fig. 8, the FT-IR spectra of the purely silicious mesoporous SBA-15 and Ti-SBA-15 samples are shown. Two peaks at 2926 and

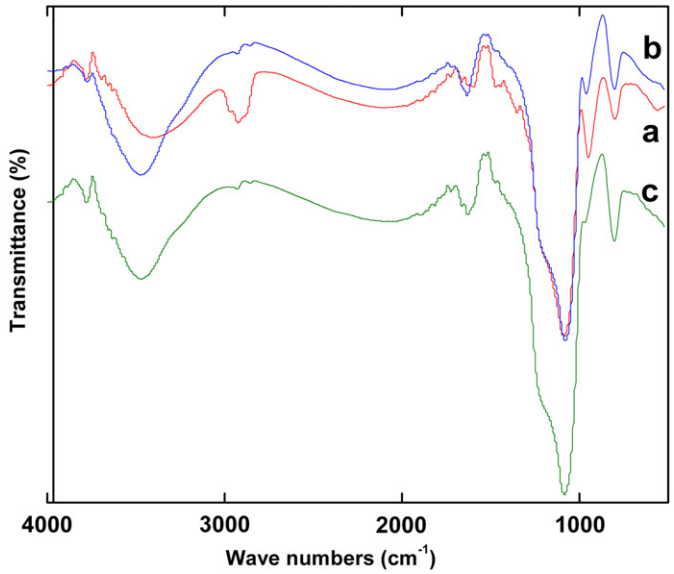

Fig. 8. FT IR spectra of as-synthesized Ti-SBA-15 (a, sample 1), calcined Ti-SBA-15 (b, sample 1) and calcined SBA-15 (c).

2856 cm^{-1} observed in the as-synthesized mesoporous Ti-SBA-15 samples could be attributed to asymmetric and symmetric C–H stretching vibrations, respectively. Disappearance of these peaks in the calcined sample indicated complete removal of the template molecule from the as-synthesized sample. Broad peak observed at 3428–3474 cm^{-1}could be assigned for O–H stretching of the defect Si–OH groups and residual water to pure calcined mesoporous SBA-15 and as well as calcined mesoporous Ti-SBA-15 samples. The absorption band at 1083 and 802 cm^{-1} are assigned to the ν_{as}(Si–O–Si) and ν_s(Si–O–Si), respectively, for calcined mesoporous Ti-SBA-15 [21]. Whereas in the pure silica mesoporous SBA-15 materials the intensity of the absorption band at ca. 960 cm^{-1} is very much weaker compared to titanium containing calcined mesoporous Ti-SBA-15. Silanol groups are always present in silica even in the absence of Ti(IV). The increase in titanium content enhanced the intensity of the silanol shoulder at 960 cm^{-1} with respect to that of the ν_{as}(Si–O–Si) band [36]. Interestingly, the Ti-containing sample shows a moderately strong peak at about 960 cm^{-1}, which is attributed to Ti–O–Si bonding, indicating that some Ti condensation occurred with the siliceous species at this stage [34]. This is in good agreement with the diffuse reflectance UV result and confirms that the Ti atoms are chemically bonded to silica [35].

3.7. Thermal analysis

In Fig. 9, quantitative estimation of the content of organic tri-block copolymer Pluronic F127 molecules in a representative as-synthesized Ti-SBA-15 sample is measured by using TGA and differential thermal analysis (DTA) under N_2 flow. With an increase in temperature the sample gradually loses weight (ca. 4.4%) up to ca. 380 K due to desorption of physisorbed water. From 380 to 590 K the sample gradually losses weight (ca. 2.9%) due to desorption of strongly bound water molecules at the surface of Ti-SBA-15. Then from 590 to 850 K the sample loses rapidly 35.5% of its weight, which is mainly due to the decomposition of the organic templating molecule pluronic F127 molecules. A broad exothermic peak centered at 753 K in the DTA plot suggested the burning of the template molecules. After that the sample loses another (ca. 2.5%) of its weight steadily till 1073 K is reached. The total loss in the temperature range 590–1073 K is ca. 38% and this could be attributed to the removal of the pluronic F127 molecules.

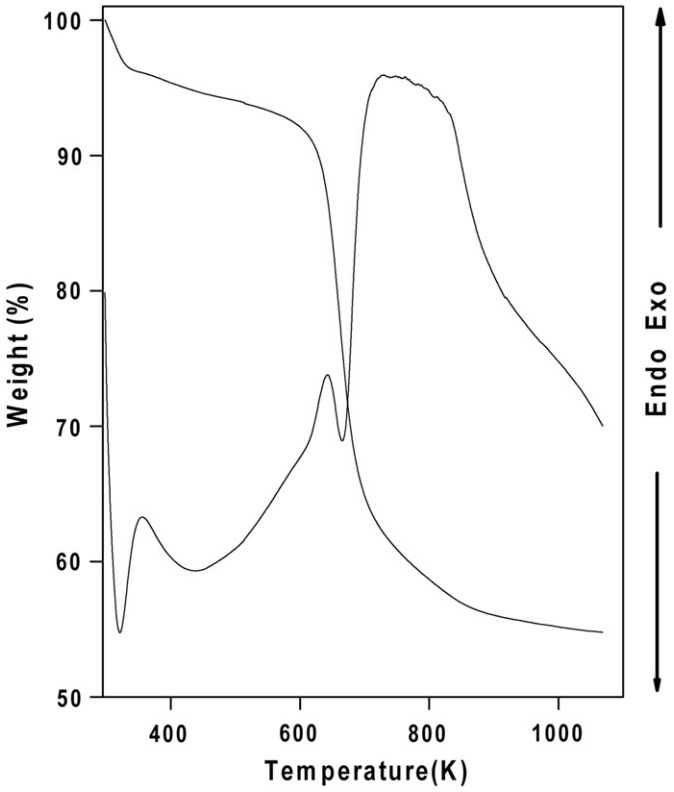

Fig. 9. Thermogravimetry (TG) and differential thermal analysis (DTA) of as-synthesized mesoporous Ti-SBA-15 (sample 1) material.

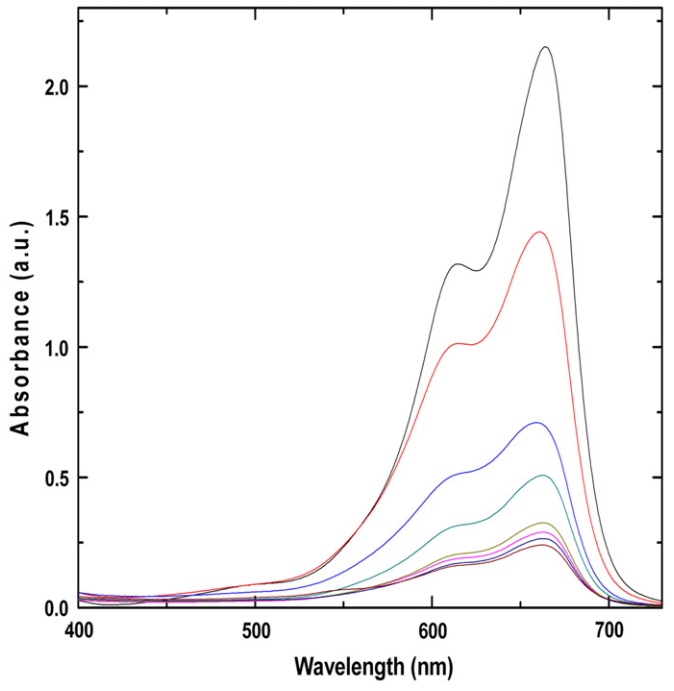

Fig. 10. Decrease absorption spectra of methylene blue (12 mg/L) in the presence of Ti-SBA-15 (sample 1) in irradiation times 0, 10, 20, 30, 60, 90, 120 and 150 min.

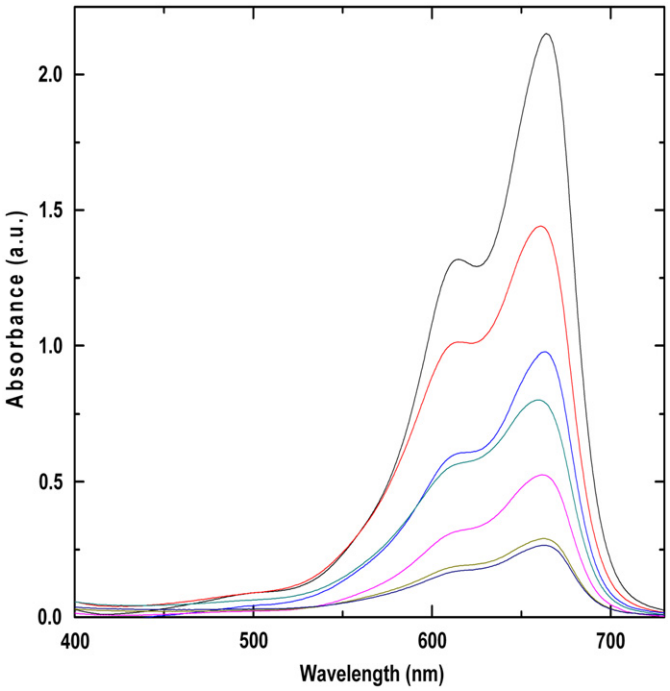

Fig. 11. Decrease absorption spectra of methylene blue (12 mg/L) in the presence of Ti-SBA-15 (sample 2) in irradiation times 0, 10, 20, 30, 60, 90 and 120 min.

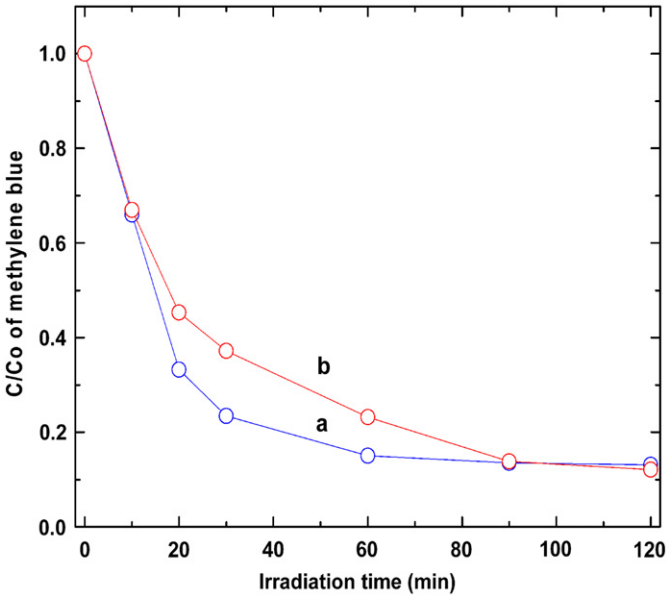

Fig. 12. Plots of concentration of Methylene Blue vs irradiation times 0, 10, 20, 30, 60, 90 and 120 min in the presence of samples 1 (a) and 2 (b), respectively.

3.8. Photodegradation of methylene blue

Being a well-known as a major pollutant of chemical plants we have studied the photodegradation of methylene blue. We have shown the catalytic efficiency of the Ti-SBA-15 materials in photodegradation of methylene blue in an environmentally benign route in Figs. 10 and 11. Before the reaction methylene blue and Ti-SBA-15 photocatalyst mixtures are taken in a beaker and stirred in dark for 60 min to get a homogeneous suspension. The stirring of solution is the essence for well adsorption of the dye to the catalyst support surface [25]. Use of higher amount of catalyst decreases the penetration depth of light because of scattering of light by the catalyst [37]. Samples have been collected within regular time intervals and collected samples are monitored by UV–visible absorption spectra regarding λ_{max} at 661 nm, the characteristic spectra (λ_{max}) of methylene blue. Figs. 10 and 11 clearly demonstrate that the absorbance (λ_{max}) of the dye decreases continuously with increase of time in presence of sample 1 and sample 2, respectively. The decolorization and degradation efficiency have been calculated by employing equation

$$D\% = \left[\frac{C0-C}{C}\right] \times 100.$$

where C_0 is the initial concentration of dye and C is the concentration of dye after irradiation in selected time interval. Fig. 12 shows the plots of concentration of methylene blue against irradiation time in the presence of sample 1 (a) and sample 2 (b), respectively. We make a comparative study for the photodegradation of methylene blue over Ti-SBA-15 with standard P25 and other reported titania incorporated SBA-15 or TiO_2 impregnated SBA-15 materials (Table 2, [38–40]). Solar photocatalytic decolorization of methylene blue in aqueous medium occurs only 10% of the initial concentration (9 mg/L) after 6 h over TiO_2 photocatalyst [41]. Here, the degradation occurs up to 89% within 150 min in presence of Ti-SBA-15 material. More specifically it has been observed that the degradation of the dye occurred up to 84.93% within 60 min but further irradiation can only lead degradation of very small extent. But when we take Ti-SBA-15 sample 2, degradation occurred up to 75.6% within 60 min and further irradiation of the samples up to 120 min led to 87.7% decomposition indicating this material is comparatively less efficient than the sample 1. We have calculated the first-order rate constant k (min^{-1}) for photodegradation of dyes by employing following equation:

$$\ln C = \ln C_0 - kt \quad (1)$$

where C_0 and C are dye concentrations initially and after time t, respectively. We calculate first-order rate constant k (0.047 and 0.038 min^{-1} for samples 1 and 2, respectively) for photodegradation of methylene blue. The rate constant (k) of P25 is 0.022 min^{-1} [40]. Higher rate constant for the decomposition of methylene blue of our synthesized materials than standard P25 materials suggested that our materials are more active than standard P25. Hence, above findings clearly demonstrate that higher amount of titanium incorporation

Table 2
Comparative study of first-order reaction rate constants (k) of different photocatalysts.

Entry	Sample type	Dye name	Rate constant k (min^{-1})	Reference
1	Sample 1	Methylene blue	4.70×10^{-2}	This work
2	Sample 2	Methylene blue	3.80×10^{-2}	This work
3	TiO_2/SBA-15	Orange II	$0.50–2.00 \times 10^{-2}$	[38]
4	30% TiO_2/SBA-15	Methylene blue	$2.40–6.90 \times 10^{-2}$	[39]
5	P25 (Degussa)	Methylene blue	2.20×10^{-2}	[40]
6	No catalyst	Methylene blue	2.26×10^{-4}	This work

into the framework of SBA-15 makes the catalyst more efficient for photocatalytic degradation of organic dyes.

4. Conclusions

Highly ordered mesoporous Ti-SBA-15 materials have been synthesized using the self-assembly of a non-ionic amphiphilic tri-block copolymer surfactant, pluronic F127 under acidic pH conditions. Characterization results suggest the highly ordered 2D-hexagonal arrangement of pores in Ti-SBA-15 materials with uniform large mesopores of dimension ca. 10.4–10.5 nm. Spectroscopic results suggested that most of the titanium sites present in these samples are tetrahedrally coordinated Ti(IV). In addition to tetrahedral coordination there is considerable extent octahedral coordination sites in the Ti-SBA-15 framework, which could result due to its synthesis under strong acidic conditions. It has been demonstrated that the silicate framework can successfully accommodate sufficient Ti-atoms without perturbing mesocopic ordering. The calcined mesoporous Ti-SBA-15 shows higher BET surface area and this is reflected in much larger H_2 uptake at higher external pressure vis-à-vis pure silica SBA-15. Our Ti-SBA-15 material showed excellent efficiency in photocatalytic degradation of methylene blue, which is largely present in industrial wastes. Thus, mesoporous Ti-SBA-15 material has potential applications in hydrogen storage and environmental clean-ups.

Acknowledgments

AB wishes to thank Department of Science and Technology, New Delhi for providing the research grant. SKD, MKB wish to thank CSIR for Senior Research Fellowships.

References

[1] C.T. Kresge, M.E. Leonowicz, W.J. Roth, J.C. Vartuli, J.S. Beck, Nature 359 (1992) 710.
[2] A.K. Sinha, K. Suzuki, Angew. Chem. Int. Ed. 44 (2005) 271.
[3] J. Jitputti, S. Pavasupree, Y. Suzuki, S. Yoshikawa, J. Solid State Chem. 180 (2007) 1743.
[4] H. Yang, D. Zhao, J. Mater. Chem. 15 (2005) 1217.
[5] Z. Han, H. Zhu, J. Shi, G. Parkinson, G.Q. Lu, J. Solid State Chem. 180 (2007) 902.
[6] M.G. Kanatzidis, Adv. Mater. 19 (2007) 1165.
[7] T.A. Zepeda, B. Pawelec, J.L.G. Fierro, A. Montesincs, A. Olivas, S. Fuentes, T. Halachev, Micropor. Mesopor. Mater. 111 (2008) 493.
[8] P. Han, H.M. Zhang, X.P. Qiu, X.L. Ji, L.X. Gao, J. Mol. Catal. A: Chem. 295 (2008) 57.
[9] Y.L. Wei, Y.M. Wang, J.H. Zhu, Z.Y. Wu, Adv. Mater. 15 (2003) 1943.
[10] K.P. Gierszal, M. Jaroniec, J. Phys. Chem. C 111 (2007) 9742.
[11] Y. Li, B. Yan, J. Solid State Chem. 181 (2008) 1032.
[12] D. Chandra, S. Mridha, D. Basak, A. Bhaumik, Chem. Commun. (2009) 2384.
[13] T. Prozorov, S.K. Mallapragada, B. Narasimhan, L. Wang, P. Palo, M. Nilsen–Hamilton, T.J. Williams, D.A. Bazylinski, R. Prozorov, P.C. Canfield, Adv. Funct. Mater. 17 (2007) 951.
[14] J. Yang, K. Hidajat, S. Kawi, Mater. Lett. 62 (2008) 1441.
[15] B.D. Alexander, P.J. Kulesza, L. Rutkowska, R. Solarska, J. Augustynski, J. Mater. Chem. 18 (2008) 2298.
[16] A. Bhaumik, T. Tatsumi, J. Catal. 182 (1999) 349.
[17] G.A. Eimer, S.G. Causscelli, G.E. Ghione, M.E. Crivello, E.R. Herrero, Appl. Catal. A. Gen. 298 (2006) 232.
[18] A. Corma, H. Garca, M.T. Navarro, E.J. Palomares, F. Rey, Chem. Mater. 12 (2000) 3068.
[19] R.J. Davis, Z. Liu, Chem. Mater. 9 (1997) 2311.
[20] M.S. Morey, S. O'Brien, S. Schwarz, G.D. Stucky, Chem. Mater. 12 (2000) 898.
[21] N.N. Trukhan, V.N. Romannikov, A.N. Shmakov, M.P. Vanina, E.A. Paukshtis, V.I. Bukhtiyarov, V.V. Kriventsov, I.Y. Danilov, O.A. Kholdeeva, Micropor. Mesopor. Mater. 59 (2003) 73.
[22] M. Sasidharan, N.K. Mal, A. Bhaumik, J. Mater. Chem. 17 (2007) 278.
[23] X. Hu, B.O. Skadtchenko, M. Trudeau, D.M. Antonelli, J. Am. Chem. Soc. 128 (2006) 11740.
[24] W. Dong, Y. Sun, C.W. Lee, W. Hua, X. Lu, Y. Shi, S. Zhang, J. Chen, D. Zhao, J. Am. Chem. Soc. 129 (2007) 13894.
[25] K.M. Parida, N. Sahu, J. Mol. Catal. A: Chem. 287 (2008) 151.
[26] A.M. Busuioc, V. Meynen, E. Beyers, P. Cool, N. Bilba, E.F. Vansant, Catal. Commun. 8 (2007) 527.
[27] D.I. Petkowicz, R. Brambilla, C. Radtke, C.D.S. Silva, Z.N. Rocha, S.B.C. Pergher, J.H.Z. Santos, Appl. Catal A: Gen. 357 (2009) 125.
[28] G. Li, X.S. Zhao, Ind. Eng. Chem. Res. 45 (2006) 3569.
[29] S. Nagak, Y. Fukushima, K. Kuroda, J. Chem. Soc. Chem. Commun. (1993) 680.
[30] F. Gao, Y.H. Zhang, H.Q. Wan, Y. Kong, X.C. Wu, L. Dong, B. Li, Y. Chen, Micropor. Mesopor. Mater. 110 (2008) 508.
[31] J. Gu, W. Fan, A. Shimojima, T. Okubo, J. Solid State Chem. 181 (2008) 957.
[32] E. Durgun, Y. -R. Jang, S. Ciraci, Phys. Rev. B 76 (2007) 073413.
[33] A.I. Acatrinei, M.A. Hartl, J. Eckert, E.H.L. Falcao, C.L.L. Daemen, J. Phys. Chem. C 113 (2009) 15634.
[34] G. Petrini, A. Cesana, G. De Alberti, F. Genoni, G. Leofanti, M. Paclovan, G. Paparatto, P. Rofia, Stud. Surf. Sci. Catal. 68 (1991) 761.
[35] A. Corma, Chem. Rev. 97 (1997) 2373.
[36] A. Bhaumik, S. Samanta, N.K. Mal, Micropor. Mesopor. Mater. 68 (2004) 29.
[37] A.L. Linsebigler, G. Lu, J.T. Yates Jr., Chem. Rev. 95 (1995) 735.
[38] W.Y. Jung, S.H. Baek, J.S. Yang, K. -T. Lim, M.S. Lee, G.-D. Lee, S.S. Park, S. -S. Hong, Catal. Today 131 (2008) 437.
[39] J. Yang, J. Zhang, L. Zhu, S. Chen, Y. Zhang, Y. Tang, Y. Zhua, Y. Li, J. Hazard. Mater. B 137 (2006) 952.
[40] M. Srinivasan, T. White, Environ. Sci. Technol. 41 (2007) 4405.
[41] W.S. Kuo, P.H. Ho, Chemosphere 45 (2001) 77.